Earth's Future

RESEARCH ARTICLE
10.1029/2024EF004424

Multi-Model Simulation of Solar Geoengineering Indicates Avoidable Destabilization of the West Antarctic Ice Sheet

John C. Moore[1], Chao Yue[2], Yangxin Chen[2], Svetlana Jevrejeva[3], Daniele Visioni[4], Petteri Uotila[5], and Liyun Zhao[2]

[1]Arctic Centre, University of Lapland, Rovaniemi, Finland, [2]State Key Laboratory of Earth Surface Processes and Resource Ecology, Faculty of Geographical Science, Beijing Normal University, Beijing, China, [3]National Oceanography Centre, Liverpool, UK, [4]Department of Earth and Atmospheric Sciences, Cornell University, Ithaca, NY, USA, [5]Faculty of Science, Institute for Atmospheric and Earth System Research/Physics, University of Helsinki, Helsinki, Finland

Abstract Heat transported in Circumpolar Deep Water is driving the break-up of ice shelves in the Amundsen Sea sector of Antarctica, that has been simulated to be unavoidable under all plausible greenhouse gas scenarios. However, Solar geoengineering scenarios remain largely unexplored. Solar geoengineering changes global thermal radiative balance, and atmospheric and oceanic transportation pathways. We simulate stratospheric aerosol injection (SAI) designed to reduce global mean temperatures from those under the unmitigated SSP5-8.5 scenario to those under the SSP2-4.5 scenario with six CMIP6-class Earth System Models. These consistently show intensified Antarctic polar vortex and sub-polar westerlies, which mitigates changes to easterly winds along the Amundsen Sea continental shelf compared with greenhouse gas scenarios. The models show significantly cooler Amundsen Sea waters and lower heat content at 300–600 m under SAI than with either solar dimming or the SSP5-8.5 unmitigated greenhouse gas scenarios. However, the heat content increases under all scenarios compared with present day suggesting that although vulnerable ice shelves would continue to thin, the rate would be lower for SAI even with SSP5-8.5 specified greenhouse gases, than for the moderate (SSP2-4.5) scenario. The simulations here use solar geoengineering designed to meet global temperature targets; interventions targeted at preserving the frozen high latitudes have also been proposed that might be expected to produce bigger local effects, but potentially deleterious impacts elsewhere. Considering the huge disruptions to society of ice sheet collapse, more research on avoiding them by intervention technology is a moral imperative.

Plain Language Summary The Amundsen Sea sector of Antarctica is important because major ice sheet outlet glaciers are at, or close to, the tipping point threshold when greenhouse gas concentrations become irrelevant to their fate. Multi-meter sea level rises are essentially inevitable once past this tipping point, forcing hundreds of millions of people to relocate (mainly in the Global South), and costing around $40 billion per year per meter of sea level rise through the rest of the century in coastal defense systems. Hence any methods that may avoid ice sheet collapse should be researched. In this article we use 6 state of the art earth system models to simulate putting aerosols into the stratosphere (mimicking volcanic eruptions), might affect the heat carried by the oceans to the vulnerable glaciers in the Amundsen Sea. The stratospheric aerosols change the winds that drive warm deep water toward the glaciers, lowering the expected melting compared with the no greenhouse gas mitigation scenario, and even the lowered emissions pledged by the international community. This result contrasts with earlier work suggesting the ice sheets were doomed and encourages more sophisticated climate system interventions scenarios targeted toward to high latitudes.

Key Points:

- We simulate the effect of stratospheric aerosol injection (SAI) and greenhouse gas scenarios on ocean heat flow in the Amundsen Sea
- SAI impacts stratospheric winds that propagate into ocean circulation changes that reduce heat flow to the ice edge
- Researching ideas, that can complement mitigation, may provide alternatives to avoid crossing damaging social tipping points

Supporting Information:

Supporting Information may be found in the online version of this article.

Correspondence to:

J. C. Moore,
john.moore.bnu@gmail.com

Citation:

Moore, J. C., Yue, C., Chen, Y., Jevrejeva, S., Visioni, D., Uotila, P., & Zhao, L. (2024). Multi-model simulation of solar geoengineering indicates avoidable destabilization of the West Antarctic ice sheet. *Earth's Future*, *12*, e2024EF004424. https://doi.org/10.1029/2024EF004424

Received 10 JAN 2024
Accepted 27 APR 2024

Author Contributions:

Conceptualization: John C. Moore
Data curation: Chao Yue
Formal analysis: Chao Yue, Yangxin Chen
Funding acquisition: John C. Moore
Investigation: John C. Moore, Chao Yue, Yangxin Chen, Petteri Uotila
Methodology: John C. Moore, Chao Yue, Yangxin Chen, Svetlana Jevrejeva
Project administration: John C. Moore, Liyun Zhao
Resources: John C. Moore
Software: Chao Yue, Yangxin Chen
Supervision: John C. Moore, Liyun Zhao
Visualization: Chao Yue, Yangxin Chen, Daniele Visioni
Writing – original draft: John C. Moore

1. Introduction

Ice shelves tend to breakup and retreat when they are exposed to increased basal melt rates via ingress of relative warm, dense deep water derived from Circumpolar Deep Water (CDW) to their grounding lines (Liu et al., 2015; Turner et al., 2017). These deep warm currents circulate around Antarctica offshore of the continental shelf break. The CDW flows closest to the ice sheet in the Amundsen Sea sector (Jacobs et al., 2011), where the CDW waters overflow the 500–600 m deep sedimentary shelf outer margin (Heywood et al., 2016) and can then penetrate far onto the continental shelf via deeply incised bathymetric channels and directly access sub-ice shelf cavities (Wåhlin et al., 2013, 2020). In the Amundsen Sea sector large glaciers are resting on bedrock that deepens inland away from their grounding lines, and which are thought to be already vulnerable to Marine Ice Shelf Instability

Writing – review & editing: John C. Moore, Yangxin Chen, Svetlana Jevrejeva, Daniele Visioni, Petteri Uotila, Liyun Zhao

(Favier et al., 2014; Joughin et al., 2014). As the buttressing force stabilizing the glaciers is reduced by ice shelf basal melting, the inland ice accelerates across the grounding line potentially leading to rapid grounding line retreat. Global sea level rises of several meters are possible if Thwaites and neighboring glaciers collapse because this would likely destabilize much of West Antarctica that presently rests on beds far below sea level (DeConto & Pollard, 2016; Turner et al., 2017).

The oceans have absorbed 93% of the increased radiative heating from greenhouse gases, and hence are a huge reservoir of energy (Trenberth and Fasullo, 2016). Any changes in ocean circulation are a concern if this supply of energy is directed toward sensitive environments—such as the West Antarctic ice sheet (WAIS). Solar geoengineering is designed to act on incoming solar radiation whereas as greenhouse gases absorb long wave outgoing radiation and the net result is spatial and temporal differences in radiative forcing that will impact, for example, equatorial-polar temperature gradients, and atmosphere-ocean circulation patterns (Gertler et al., 2020; Xie et al., 2022). Despite this, simulations of impacts of solar geoengineering show global benefits in moderating temperature rise compared with the impacts expected under modest greenhouse gas forcing scenarios such as SSP245, and unmitigated scenarios such as SSP585 (Harding et al., 2020; Irvine & Keith, 2020).

There have been three previous studies of SRM impact on WAIS (Table 1). Two recent studies on the simulation of the impacts of geoengineering on the stability of the WAIS contrast with early work (McCusker et al., 2015) that concluded that SAI would promote warm water flows to the vulnerable ice shelves, destabilizing the ice sheet. Sutter et al. (2023) show that on a high-GHG pathway, solar geoengineering to designed to limit global mean temperatures rises to 1.5°C would only be effective at stabilizing WAIS if started immediately (2020), whereas on an intermediate GHG pathway, SAI from mid-century may be effective. While, Goddard et al. (2023) use a suite of stratospheric sulfate aerosol injection (SAI) simulations at different latitudes to show that collapse depends on aerosol injection strategy, with greater cooling of key waters adjacent to the vulnerable ice shelves if the southern hemisphere were preferentially targeted. Recent greenhouse gas only simulations driving a high resolution ocean model of Amundsen Sea found accelerated ice shelf melt rates under every future climate pathway (Naughten et al., 2023), implying that mitigation was no longer a viable option to prevent ice sheet collapse. In contrast with previous studies on interventions that relied on climates from single models (Table 1), in this paper we simulate SAI designed to reduce global mean temperatures from those under an unmitigated emissions scenario to those under a more moderate scenario that more closely tracks the Paris 2015 multi-country emissions pledges, with six CMIP6-class Earth System Models.

2. Data and Methods

In this article we consider the impacts on the Amundsen Sea with six state of the art climate models in contrast with single model studies that have been used earlier (Table 2) and we consider here both the largely theoretical concept of solar dimming geoengineering by which the solar constant is lowered, mimicking the idea of a space parasol, and the more practical SAI method, mimicking volcanism.

SSP245 is a mid-range greenhouse gas scenario where radiative forcing peaks in mid-21st century and global mean temperatures rise throughout the century before cooling in the 22nd and SSP585 is a no mitigation scenario where radiative forcing and temperatures continue to rise throughout the 21st century (O'Neill et al., 2016). The geoengineering simulations we use here are the GeoMIP6 (Geoengineering Model Intercomparison Project; Visioni et al., 2023), G6solar and G6sulfur. G6solar (Kravitz et al., 2015) is a solar dimming experiment where

Table 1
Previous Studies of Antarctic Response to Solar Radiation Management (SRM)

Study	Climate models	SAI injection	Target GMT-PI	GHG scenario	Anomalies versus baseline	SRM window
McCusker et al. (2015)	CCSM4	Tropical	1	RCP8.5	2045–54 versus 1970–1999	2035–2100
Sutter et al. (2023)	HadGEM2-ES	Tropical	1.5	RCP8.5, 4.5, 2.6	Range versus 1995–2014	2020–3000
Goddard et al. (2023)	CESM2-WACCM6	30°N, 15°N, Eq, 15°S, 30°S	0.5, 1,1.5	SSP245	2050–69 versus 1990–2009	2035–2069
This study	6 ESM (Table 2)	Tropical	SSP245	SSP585	G6 versus SSP585	2020–2100

Note. The climate models describe the ESM model analyzed, the SAI strategy used and the targeted global mean temperature relative to pre-industrial levels (GMT-PI), or SSP scenario, anomalies are the experiment period and control used in the analyses, and the SRM window is the duration of the SRM forcing.

Table 2
The Earth System Models Used Here

Model	r[a]	ECS[b]	Ocean resolution × layers	Atmosphere resolution	Stratospheric aerosols in G6sulfur (AOD, injected SO_2 Tg SO_2/yr during 2081–2100 or 2089)[c]	References
CESM2-WACCM	2	4.7	320 × 384 × 60	192 × 288	Inject SO2 at the equator at 25 km altitude, rate change for every decade. (0.296,21)	Gettelman et al. (2019)
CNRM-ESM2.1	3[d]	4.8	362 × 294 × 75	256 × 128	AOD scaled from Tilmes et al. (2015), rate change for every year. (0.327, na)	Séférian et al. (2019)
IPSL-CM6A-LR	1	4.6	362 × 332 × 75	144 × 143	Inject SO_2 between 10°N and 10°S with 18–28 km of altitude, rate change for every decade. (0.363, 40)	Boucher et al. (2020)
MPI-ESM1.2-HR	3	3.0	802 × 404 × 40	384 × 192	AOD scaled from Niemeier and Schmidt (2017), rate change for every year. (0.235,36)	Gutjahr et al. (2019)
MPI-ESM1.2-LR	2	3.0	256 × 220 × 40	192 × 96	AOD scaled from Niemeier and Schmidt (2017), rate change for every year. (0.235,36)	Mauritsen et al. (2019)
UKESM-1.0-LL	1	5.3	360 × 330 × 75	192 × 144	Inject SO_2 between 10°N and 10°S with 18–28 km of altitude, rate change for every decade. (0.357,21)	Sellar et al. (2019)

Note. Time spans in G6solar and G6sulfur for MPI-ESM1.2-LR and MPI-ESM1.2-LR are available in 2020–2089. We bi-linearly interpolated each ESM to a common grid of 0.5° × 0.5° resolution to facilitate multi-model ensemble mean calculation. [a]We use all the ensemble members available in each ESM for both historical and future scenarios and weight all ESM equally in the ensemble mean. [b]Equilibrium climate sensitivity from Meehl et al. (2020), with mean of 4.2 ± 1°C. [c]Data from Visioni et al. (2021), na means not available. [d]Only 1 realization was available for G6solar.

greenhouse gas forcing follows the SSP585 scenario, but incoming shortwave radiation is lowered from 2020 so that global mean top of atmosphere radiative forcing matches closely to the SSP245 scenario which is close to the mitigation commitments agreed towards the Paris 2015 accord (Kitous & Keramidas, 2015). G6sulfur (Kravitz et al., 2015) also reduces SSP585 radiative forcing to SSP245, but using SAI into the lower tropical stratosphere, again starting in 2020 and running until 2099. In fact, several models only have data until 2089. In our analysis we compare the available final 20 years of geoengineering (2070–2089) in the different scenarios, with SSP585 as the reference since we are concerned how the scenarios reverse or avoid the large greenhouse gas forced changes in SSP585. All four scenarios used produce higher radiative response than at present until mid-century, and consequently show increases in surface temperature (Visioni et al., 2021) and sea level rise (Yue et al., 2023). The simulations here do not reach any steady state, and Sutter et al. (2023) show that the ice sheet response continues for many centuries, but air and continental shelf ocean temperatures respond far faster, so that useful inferences may be made with simulations just for the 21st century (e.g., Goddard et al., 2023; McCusker et al., 2015).

These simulations have been done by six CMIP6 generation earth system models (ESM; Table 2; Visioni et al., 2021). CMIP6 models significantly improve Southern Ocean simulation quality, especially in realism of wind driven transports compared with earlier generation models (Beadling et al., 2020). The CCSMv4 model used by McCusker et al. (2015) was of similar resolution to the six ESMs we use (Table 2), but it was two model generations earlier than the CESM2 we use; similarly the HadGEM2-ES used by Sutter et al. (2023) is a CMIP5 generation model of reduced complexity compared with its CMIP6 successor, UKESM-1, that we use here (Table 2). Southern Ocean simulations have large model spread, but significant changes in wind speed occur under both greenhouse gas scenarios and solar geoengineering (Gertler et al., 2020; Wei et al., 2018). Thus, the most robust estimates of stratospheric to surface winds and ocean temperatures will come from a multi-model ensemble of CMIP6 generation models, and here we use all available realizations of the G6 experiments (Table 2) with matching realizations for SSP scenarios.

The 6 ESM (Table 2) tend to the "hot" in terms of their equilibrium climate sensitivity. Hausfather et al. (2022) suggest only using models which fall in the likely range of ECS 2.5–4°C (thereby excluding all but 2 ESM here), or within the very likely range of 2.3–4.7°C, excluding 2 out of 6 models. These high ECS may be erroneous, but we do not observe especially different behavior of these "hot" models in the particular anomaly fields we

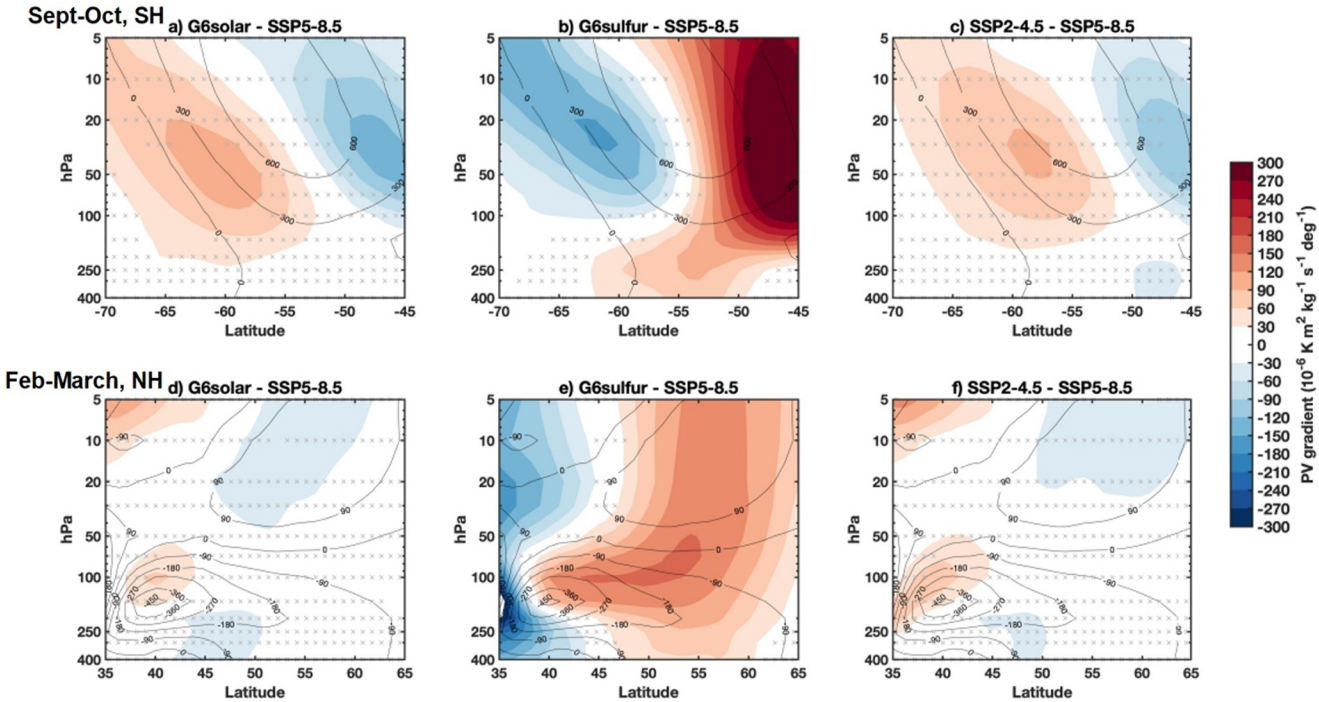

Figure 1. 6-ESM ensemble mean spring time (Sep–Oct and Feb–Mar) anomalies in Ertel's potential vorticity gradient in the atmosphere across southern (a–c) and northern (d–f) mid to high latitudes under SSP585, G6solar and G6 sulfur experiments relative to SSP585. Contour lines indicate the background potential vorticity gradient in SSP585. Stippling indicates places where anomalies are insignificant at the 95% level. Individual ESM are in Figure S1 in Supporting Information S1.

examine, and so we decide to keep all ESM in the ensemble results. Some details of the aerosol injection strategy for G6sulfur are listed in Table 2, and a discussion of the various methods for simulating the SAI can be found in Visioni et al. (2021) along with the comparison of ESM with the 1991 Mt. Pinatubo eruption. The G6sulfur specifies tropical injection and all 6 ESM have higher concentrations in the tropical stratospheric pipe than at higher latitudes as observed with Pinatubo, although with wide model spread. The quantity of aerosol needed to reduce SSP585 to SSP245 radiative forcing in the last decades of simulation is 29 ± 9 Tg SO_2/yr (Table 2), which indicates a measure of the cross-model differences in aerosol model physics.

The sub-100 km scale details of Antarctic continental shelf bathymetry are not resolved in ESMs, but what we can examine is the thermal structure of waters near the 500–600 m deep shelf break (Heywood et al., 2016; Hogan et al., 2020). The draft of Thwaites ice shelf and Pine Island Glaciers are about 300–500 m (Morlighem et al., 2020), while the depth of the thermocline is at 200–700 m (Heywood et al., 2016), hence temperatures of waters in the 300–600 m depth range are the most critical in assessing changing thermal impacts on glacier grounding lines in the Amundsen Sea sector.

3. Results

SAI by design involves introducing radiatively active components to the atmosphere, and sulfate has been widely simulated since it produces global cooling after large volcanic eruptions (Robock, 2000). However, the radiative effects of sulfate aerosol also produces stratospheric heating (Visioni et al., 2020), and various chemical reactions that are expected to deplete stratospheric ozone (Tilmes et al., 2022). SAI in models leads to an intensification of the spring time polar vortex (Visioni et al., 2020), especially over Antarctica (Figure 1), whereas projections of changes to the vortex under future global warming scenarios are more uncertain since ozone recovery rates will play a key role (Eyring et al., 2013).

Changes in ocean circulation are driven by surface winds, which can in turn be driven by downward propagation of stratospheric anomalies (Baldwin & Dunkerton, 2001). Intensification of the polar stratospheric vortex occurs most clearly under the G6sulfur experiments relative to G6solar (Figure 1). This is especially noticeable in the polar spring. There is clear similarity between G6solar and SSP2-4.5 in both northern and

10.1029/2024EF004424

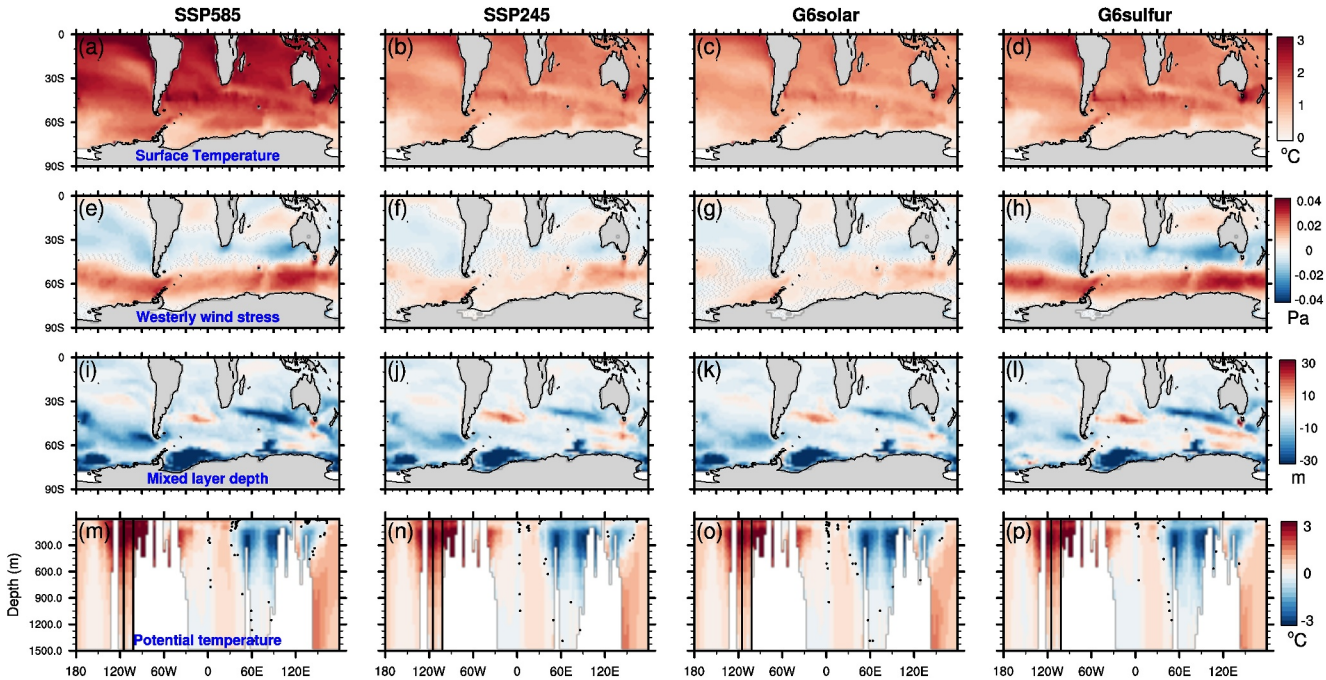

Figure 2. 6-ESM ensemble mean southern hemisphere climate anomalies relative to 1995–2014 for the four scenarios: SSP585, SSP245, G6solar and G6sulfur. Top row (a–d) shows sea surface temperatures, second row (e–h): westerly wind stress; third row (i–l): mixed layer depth and fourth (m–p) row: potential temperatures in the top 1500 m of the Southern Ocean as a function of longitude at 66°S. The Amundsen Sea sector is marked with black lines on the bottom row (102–115°W) Stippling indicates places where anomalies are insignificant at the 95% level. Individual ESM results are in Figure S2 in Supporting Information S1.

southern spring, which may be surprising considering the differences in radiative forcing between greenhouse gas and solar dimming. Part of the change in vortex with SAI is due to stratospheric ozone depletion, but it is mainly a response to the changing thermal balance in the global stratosphere (Visioni et al., 2020). The induced strengthening and expansion equatorward of the polar vortex leads to increases in tropospheric winds, in particular the surface westerly winds in the Southern Ocean (Figure 2h), although model spread means localized impacts can vary. Impacts in the Arctic are much smaller because of the geographic placement of the Arctic Ocean and surrounding land masses compared with the high-elevation Antarctic continent and surrounding Southern Ocean.

Sea surface temperatures will rise in all climate scenarios relative to the recent past (Figure 2). Westerly wind stresses also exhibit increases in the Southern Ocean relative to historical times in all scenarios, while mixed layer depths decrease in consequence (Figure 2, second and third rows). Potential temperatures at 66°S show strongest warming in the Amundsen and Bellingshausen Seas (around 100°W) and cooling in the Prydz Bay, Amery ice shelf sector (around 80°E; Figure 2, bottom row). Differences between the SSP585 and the other three scenarios in surface temperature are obvious (Figure 2). By design the G6 scenarios match the global mean temperatures in SSP245, and in general the spatial patterns are similar. There are more obvious differences in surface winds between the G6 scenarios, with G6solar similar to SSP245, and G6sulfate closer to SSP585 in the Southern Ocean.

Figure 3 compares the scenario anomalies relative to SSP585. While there are few obvious difference between the G6 anomalies in sea surface temperatures, the westerly winds under G6sulfate in the Southern Ocean are clearly different from the G6solar anomalies (Figures 3g and 3h). Potential temperatures deeper than 300 m are warmer in G6solar than SSP585 (Figure 3j), while they are cooler under G6sulfate. The potential temperatures in the Amundsen Sea sector deeper than 300 m are even cooler than under SSP245 all around Antarctica (cf Figures 2n and 2p).

In the Southern Hemisphere, the accelerated westerlies under all scenarios, but most visibly in all ESM (Figure S2 in Supporting Information S1) under SSP585 (Figure 2e) and G6sulfur (Figure 2h), in combination with the Coriolis force increases the northward Ekman transport in the upper ocean. Changes in the Ekman transport result in

10.1029/2024EF004424

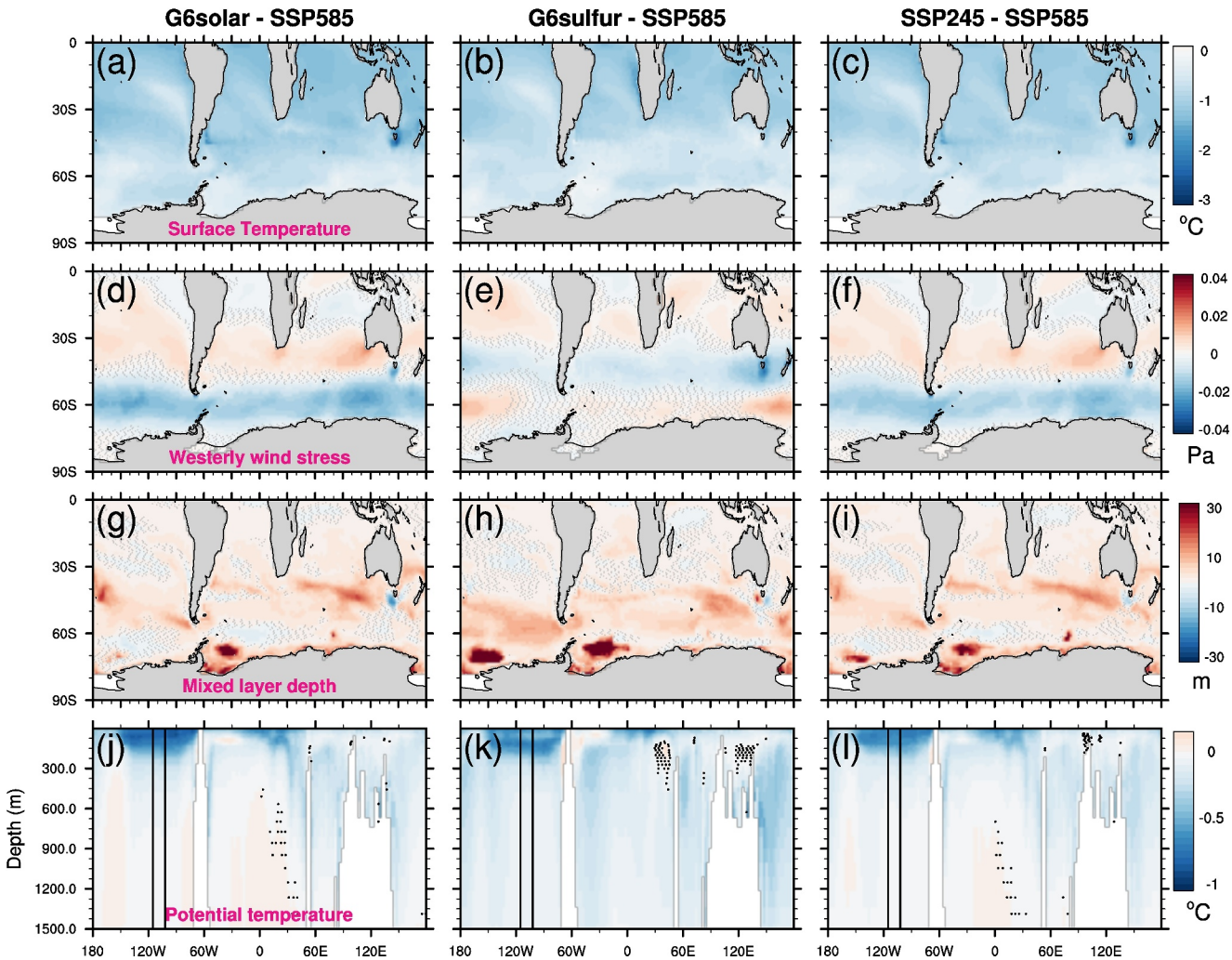

Figure 3. The six model ensemble southern hemisphere mean anomalies relative to SSP585 during the years 2070–2089, of: (a–c) Surface temperature; (d–f) Westerly surface wind stress; (g–i) Mixed layer depth (m) changes; (j–l) Potential temperatures in the top 1,500 m of the Southern Ocean as a function of longitude at 66°S. The Amundsen Sea sector is marked on the bottom row (102–115°W) Stippling indicates places where anomalies are insignificant at the 95% level. Individual ESM are in Figure S3 in Supporting Information S1.

geostrophic adjustments that lead to changes in regional sea level, for instance due to the poleward migration of the Antarctic convergence (Rintoul & Naveira Garabato, 2013). Hence, the G6solar and SSP245 sea level anomalies relative to SSP585 are larger (Figures 4a and 4c) than the G6sulfur anomaly (Figure 4b), which produces a fall in sea level around the Antarctic coast in 5 of 6 ESM (Figure S4 in Supporting Information S1), with the UKESM being slightly exceptional, but still with lower rise than G6solar or SSP245 relative to SSP585. Importantly, the continuity of fluid volume dictates that deep waters, such as CDW, upwell under G6solar and SSP245 (Figures 4d and 4f) to compensate for the increased northward upper ocean Ekman transport (Figures 4g and 4i).

This deep-water upwelling might be expected to increase temperatures offshore of the Antarctic continental break, but we see significant cooling in water temperatures in the upper 300 m of waters at 66°S (Figures 3j and 3l). These waters are shallower than CDW, and called Antarctic Surface Water (ASW), which under some conditions are entrained in the Antarctic Circum-Polar Current and gain access to the sub-ice shelf cavities (Jenkins et al., 2016), furthermore these waters are expected to be most sensitive to surface wind conditions. Indeed, in the Amundsen Sea there is greater than average cooling under both G6solar (Figure 3j) and G6sulfur (Figure 3k) compared with the rest of the 66°S meridian. Only in the Weddell Sea is there any degree of warming under G6solar relative to SSP585, where there are also corresponding increases in mixed layer thickness and surface temperatures (Figures 3a–3g).

10.1029/2024EF004424

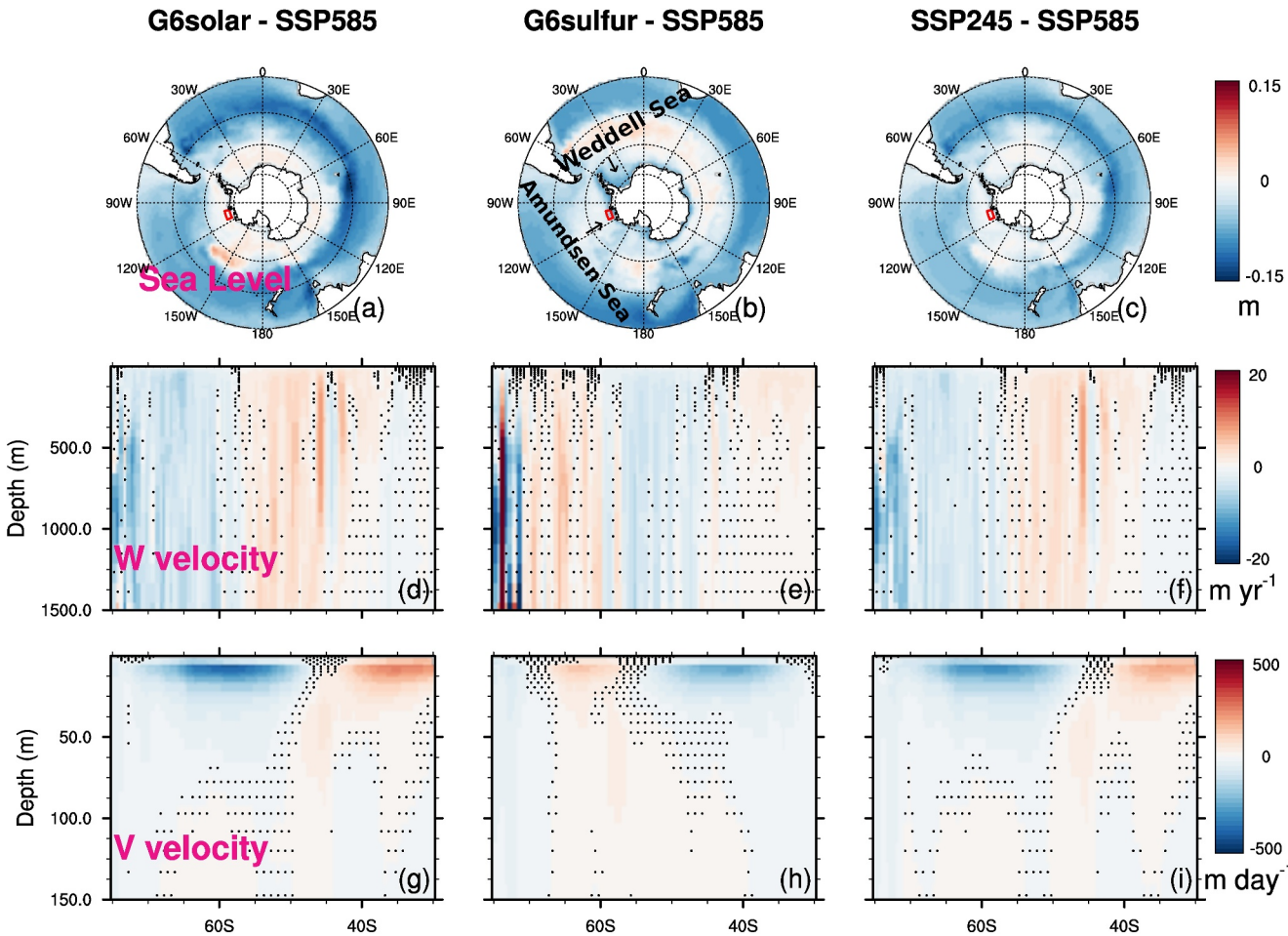

Figure 4. The six model ensemble zonal (30–75°S) mean anomalies relative to SSP5.85 in the Southern Ocean, of: Panels (a)–(c) Regional sea level due to thermosteric and dynamic effects (no data for CESM2-WACCM); (d–f) vertical velocity in the upper 0–1,500 m; (g–i) Meridional velocity in the upper 150 m. Currents almost everywhere in all scenarios in the same direction and positive (red) anomalies indicate more upwelling or northerly flow. Region used to calculate Figure 5 relations is marked by the red box in the Amundsen Sea in panels (a)–(c). Stippling indicates places where anomalies are insignificant at the 95% level. Individual ESM are in Figure S4 in Supporting Information S1.

Visioni et al. (2021) compared the surface temperature response of the 6 ESM and scenarios we use here. They found a general residual warming pattern over Eurasia and the Arctic particularly in G6sulfur, and modest relative overcooling of the tropics relative to SSP245. This is explained by stratospheric heating from the SAI, in addition to long-observed tropical responses (Govindaswamy et al., 2003) to differences in seasonal and vertical profiles of warming from greenhouse gases and year-round equatorial SAI. The cooling equatorward of 30° under G6solar is 1.16 (Figure 3a; model range 1.03 (CNRM-ESM2-1) to 1.28 (MPI-ESM1-2-HR) and 1.3 under G6sulfur 1.3 (range 1.02 (CNRM-ESM2-1) to 1.99 (MPI-ESM1-2-LR); (Figure 3b) times the extra-tropical region (Figure 3c).

The relative cooling of the tropical oceans is important because conditions there are statistically better correlated with Amundsen Sea ice shelf episodes of retreat and advance than purely regional drivers (Holland et al., 2019). Changes in ice shelf melt rate due to water import onto the continental shelf are correlated with the extra-tropical response of ENSO that brings westerly air flow over the shelf edge (Holland et al., 2019). The G6 experiments by design reduce the energy absorbed by the oceans with both G6 experiments reducing SSP585 surface temperature anomaly fields close to those under SSP245 (Figures 2 and 3). Thus, on long timescales oceans heat up at a much slower rate than under SSP585, and hence the oceans around Antarctica would never reach temperatures that they would under SSP585 as long as the interventions were to continue, or eventually atmospheric greenhouse gases had been reduced.

4. Discussion and Conclusion

The temperatures in the 300–600 m depth range at 66°S cool by a few tenths of degree by 2090 in all ESM under G6sulfur, and with more consistency (Figure S3 in Supporting Information S1) than either G6solar (3 from 6) or SSP245 (4 from 6) relative to SSP585. A cooling of 0.1°C can thicken an Antarctic ice shelf by 1 m/year (Rignot & Jacobs, 2002), although a sophisticated ice/ocean model would be required to adequately quantify melt for any particular glacier. The only study to date with a relatively high resolution ice dynamics model driven by from HadGEM2 when forced by the RCP8.5 (comparable with SSP585) emissions scenario leads to eventual collapse of the vulnerable parts of the WAIS after the year 2300 (Sutter et al., 2023). Only low emissions scenarios and early SRM interventions (2020 for RCP 8.5; 2040 for RCP 4.5) stabilize the ice sheet (Sutter et al., 2023). Tipping point behavior, that is irreversible hysteresis in the response of the WAIS to temperature rises is thought to occur for global mean near surface air temperature (GMT) rises of 1.5°C above pre-industrial (Armstrong Mackay et al., 2022 and references therein). This is the closest tipping point to present day conditions, and some parts of the WAIS may have already entered the unstable ice dynamical regime known as marine ice sheet instability (MISI; Schoof, 2007) whereby loss of mechanical buttressing from ice shelf thinning leads to unstable retreat when the ice sheet grounding line rests on a retrograde sloping bed (Favier et al., 2014; Joughin et al., 2014; Rignot. et al., 2014). This critical thinning of ice shelves is exclusively driven by oceanic thermal forcing in the Amundsen Sea since temperatures are not yet warm enough for any significant surface melt. Hence the oceanic thermal forcing can be viewed as a proxy for WAIS stability if a threshold temperature can be established (Armstrong Mackay et al., 2022). Sutter et al. (2023) demonstrate in their Figure 1 that in their ice model, and driven by a single ESM, the WAIS collapse likelihood dramatically increases when ocean temperatures between 400 and 700 m depths around the Antarctic ice fronts rise by 1–1.5°C above those at the end of the 20th century. Note that this water temperature rise is coincidentally the same value as the tipping point GMT threshold from Armstrong Mackay et al. (2022). Figure 2 shows that ocean temperatures rise under all 4 scenarios by more than this offshore of the Amundsen Sea continental shelf. In contrast Figure 5 shows much smaller temperature rises around all Antarctica at the 300–600 m ocean depths (Figure 5c), and also in the specific region relevant for ice sheet collapse in the Amundsen Sea (Figure 5d), at least as far as the simulations extend, to 2089. This threshold is likely model dependent but it is clearly different for the 6 models analyzed here than for the HadGEM2 model in Sutter et al. (2023).

The cooling in Figure 3 contrasts with previous experiments using a single ESM with much higher levels of greenhouse gas and SAI (McCusker et al., 2015) which found SAI produced a 0.5°C rise in the Amundsen Sea sector at depths of 200–500 m. McCusker et al. (2015) also found that solar dimming reduced temperatures at the same locations by 0.5°C relative to those in 2035 when their SAI began. The change in deep water temperatures we see may be driven by 21st century differences in radiative forcing directly since winds do affect the upper 1 km of the ocean (Vallis, 2017) and all 6 ESM simulate cooler deeper waters (300–600 m) under G6sulfur than the other scenarios.

Both the McCusker et al. (2015) and the Sutter et al. (2023) results were reconciled with the Goddard et al. (2023) simulations by consideration of the global mean near surface temperatures targets they aim for, and the injection strategy used (Table 1). Injections in both articles start when surface temperatures are already above 1.5°C above pre-industrial. Sutter et al. (2023) explicitly target 1.5C above per-industrial and McCusker et al. (2015) aims to stabilize at 2035 temperatures. Injection is tropical in these simulations, as it is in the G6sulfur scenario explored here. Goddard et al. (2023) show that reduced warming around the Antarctic coastal waters can be achieved with southern hemisphere preferential injection strategies. Sutter et al. (2023) show with a very long simulation (to the year 3000) that the only scenarios that may (with about 2:1 odds) prevent WAIS collapse are where SAI is started early (2040) and GMT is kept to about 1.5°C above pre-industrial. Goddard et al. (2023) show that the odds might be greatly increased with lower temperature targets, for example, below the temperatures at the start of the deployment, and with an early start to minimize temperature rises in the key CDW waters that access the ice shelf cavities fed by the Amundsen Sea.

In addition to water temperatures, CDW (or modified CDW) salinity changes impact density more than temperature in cold waters. Cooler surface temperatures also increase sea ice production and salt rejected which could trigger convection and deeper mixed layers. Moreover, any changes in CDW flux onto the continental shelf will impact ice shelf melt rates. Processes involved are far from understood and many are unresolvable with the ESM analyzed here, such as onshore transport in bottom Ekman layers and the topographically steered undercurrent

10.1029/2024EF004424

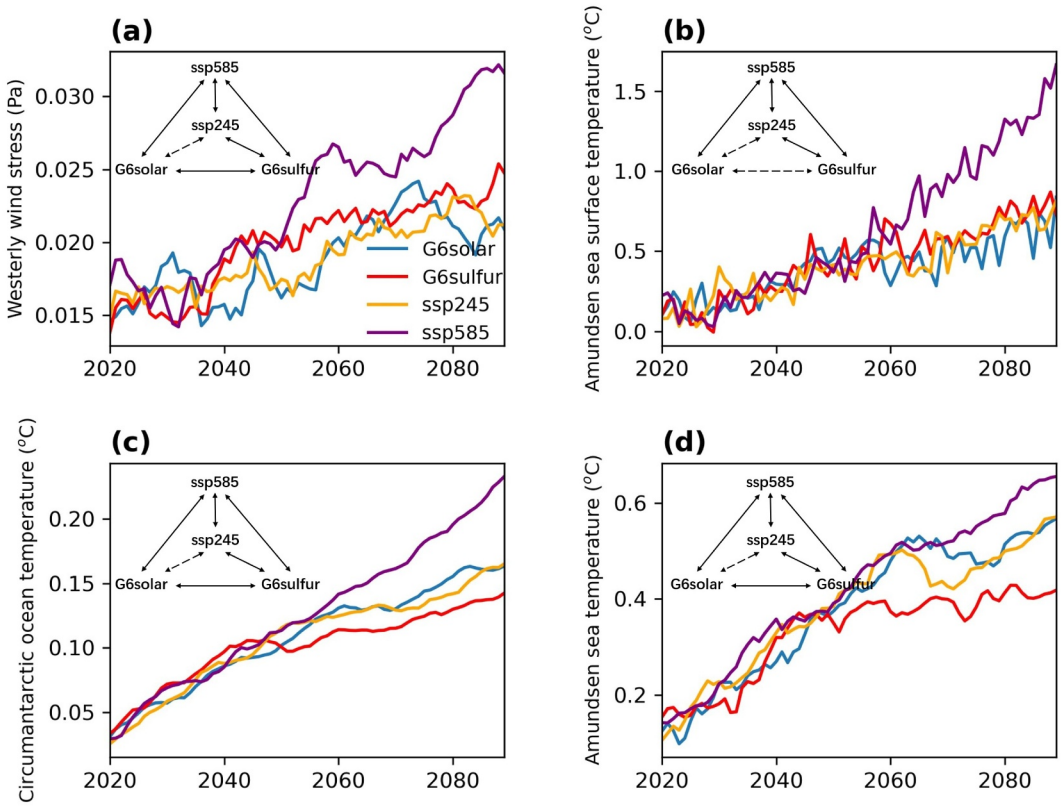

Figure 5. The six model ensemble 10-year smoothed mean time series of ocean properties anomalies relative to 1995–2014. (a) westerly wind stress in the Amundsen Sea (defined as 70–72°S by 102–115°W); (b) Amundsen Sea surface temperature; (c) temperatures at 300–600 m depth in the ocean off the circum-Antarctic continental shelf; (d) Amundsen Sea 300–600 m depth temperatures, for each of the four scenarios for all months. The inset shows the Wilcoxon paired rank differences significant at 95% as solid arrows, with dotted arrows denoting insignificantly different pairings. Individual ESMs are in Figure S5 in Supporting Information S1.

(Heywood et al., 2016). However, observations and high-resolution model analyses highlight the importance of easterly winds at, and north of, the shelf break, especially in Antarctic spring (Assmann et al., 2013; Dotto et al., 2019; Holland et al., 2019; Spence et al., 2014; Thoma et al., 2008; Walker et al., 2013), when the impact of the polar vortex circulation imposed by SAI is most intense (Figure 1).

Easterlies near the Amundsen Sea shelf break have weakened over the twentieth century (Holland et al., 2019), which has favored the driving of deep waters onto the shelf via Rossby wave teleconnections to the extra tropical Pacific on decadal scales (Holland et al., 2019). All models here, except CNRM-ESM2.0, simulate under all four scenarios strengthened westerlies, associated with the weakened easterlies. Specifically, the weakened easterlies reduce the speed of the westward geostrophic coastal flow at the surface, decrease the Ekman transport of cold Antarctic Surface Water (ASW) and its downwelling against the coast, weaken the Antarctic Slope Front, and as a result the warm CDW advances further toward the ice shelf (Jenkins et al., 2016; Figure 6). Moreover, Azaneu et al. (2023) suggest that on-shore heat flux drives melt whereby an eastward wind anomaly drives a barotropic acceleration of the eastward geostrophic undercurrent by changing the meridional sea surface slope between the shelf and offshore. In support to these arguments, westerly wind anomalies in the region are well correlated with surface temperatures in the tropical and extra-tropical Pacific (Holland et al., 2019), and historically these warm incursions have led to increases in ice shelf melt rates even without an increase in CDW temperatures (Holland et al., 2019).

Ensemble annual mean monthly wind stresses under the scenarios in the region adjacent to the shelf break are statistically different for each scenario except between SSP245 and G6solar (Figure 5), with largest westerlies under SSP585, while the other three scenarios show much smaller trends toward increased westerlies. The time series of 300–600 m ocean temperatures in the region just off the continental shelf break (Figure 5d) shows clear

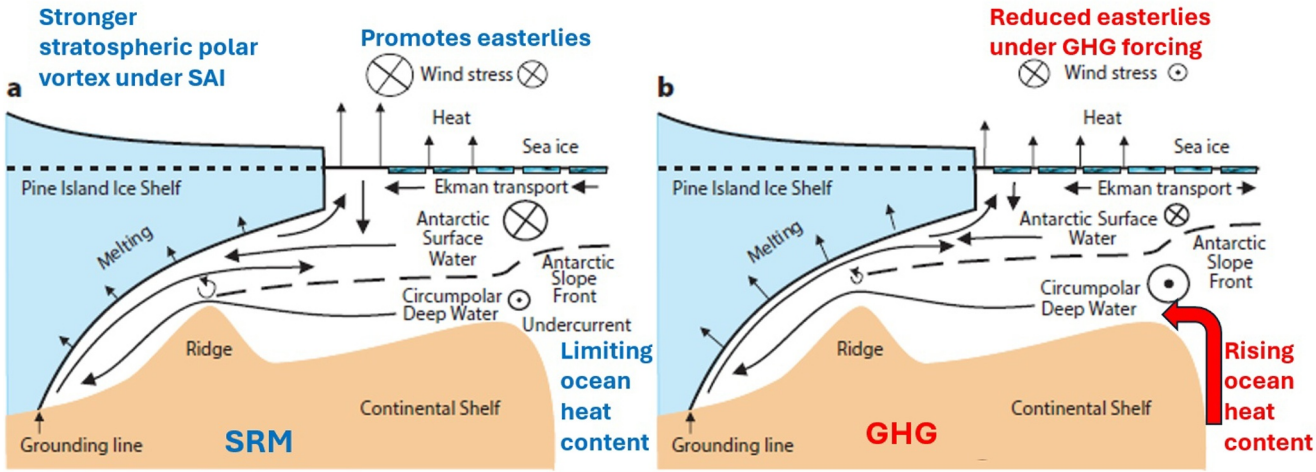

Figure 6. Schematic of processes under SRM that lead to cooler conditions (a) and under greenhouse gas forcing alone that lead to warmer conditions (b), modified after Jenkins et al. (2016). The key process allowing warm deep waters in the CDW into the ice shelf cavity is the easterlies that are promoted by the strengthened polar vortex under SAI which enhances downwelling, lowers the thermocline (the dashed line) and suppresses the Antarctic Slope Front undercurrent bringing CDW through Pine Island Trough. These processes are presently controlled from the tropical Pacific Ocean. SRM suppresses the GHG induced increases in thermal ocean forcing. All scenarios predict increases in westerlies over the Amundsen Sea, that further promote warming conditions in the sub-shelf cavities, but G6sulfur has smallest increases in westerlies due to its enhanced polar vortex from stratospheric heating.

separation between scenarios, especially after 2060, despite CESM2(WACCM) displaying only small heat content changes, all models indicate significant differences between G6sulfur and SSP585. G6sulfur has the lowest simulated ocean temperatures, while SSP585 has the largest. All scenarios show higher sea surface and 300–600 m ocean temperatures by 2050 than at present, but G6sulfur is the only scenario where the 300–600 m temperatures slow their rate of increase, potentially plateauing at about 0.3°C warmer than 2020 levels, with both SSP245 and G6solar continually rising until end of century. So, the combination of reduced temperatures in the waters offshore of the continental shelf together with lower ocean temperatures at the shelf break would likely lead to reduced melting under the G6sulfur scenario compared with SSP585, and probably SSP245.

The driver for the changing surface winds is ultimately the globally applied SAI which overcools the tropical regions relative to the poles and strengthens polar vortex (Figure 6). The resulting reduction in the pole-equator temperature gradient should preferentially reduce the wind variability near the continental shelf break in the Amundsen Sea, but may also affect for example, teleconnection patterns (Rezaei et al., 2023). Low-latitude injections of sulfate in the CESM model (Visioni et al., 2020) change the thermal wind balance due to localized heating, increasing the equator-to-pole horizontal temperature gradient in the stratosphere and strengthening the polar vortex in both hemispheres. Such strategies (like G6sulfur) would therefore make it difficult to specifically cool the polar regions by SAI. However, injections at 60°N and S may cool the high latitudes and avoid heating the tropical stratosphere to the same extent (Lee et al., 2021). Hence, surface wind impacts will be SAI strategy-dependent and CDW flux depends on local conditions and processes acting on various time scales; topography, winds, oceanic fronts and water masses.

This study is but a small step to researching alternative ideas that might contribute to the accepted paradigm of greenhouse gas mitigation. Indeed, if MISI is already underway then greenhouse gas concentrations are not relevant at any concentration because the ice sheet is then just undergoing a geometrically driven collapse that can only be arrested by additional buttressing (Schoof, 2007). Our study has several weaknesses: (a) simulations are only 70 years long; (b) with relatively low resolution; (c) are not coupled to a dedicated ice sheet model. Coupled ice-ocean simulations have recently been designed (e.g., Gladstone et al., 2021) that can capture more of the physical processes than the relatively simplified model employed by Sutter et al. (2023) which explored a wide space of ice sheet response on long timescales. Fully coupled ice-ocean models that include the boundary layer physics needed at the grounding line where the ice sheet goes afloat may need vast computing resources given the ice sheet requires resolutions of order 1 km and the ocean must be simulated (at least theoretically) on time steps of only several minutes and horizontal resolutions of tens of meters, across regions as large as many countries (Durand et al., 2011; Gladstone et al., 2021). Additionally, only very sparse data exists on ocean currents and

thermal forcing in the Amundsen Sea that drives ice shelf thinning (Wåhlin et al., 2020), and collecting such data is both expensive and hampered by very bad weather even for Antarctica (Turner et al., 2017). The calving process is critical for understanding rates of ice shelf collapse but remains one the huge challenges to ice dynamics models since cracking happens at the speed of sound and needs to be incorporated in models along with viscous deformation and sliding that is about 7 orders of magnitude slower (Benn et al., 2022).

We are not advocating for any interventions as simulated to be started; immediate and massive greenhouse gas emissions cuts must be done to preserve vital elements of the global system (Wieners et al., 2023). Instead, we want to draw attention to the possibility that there may be other options for prevention of ice sheet collapse in addition to greenhouse gas scenarios. Those alone are no longer sufficient to maintain the stability of the vulnerable ice shelves in the Amundsen Sea (Armstrong McKay et al., 2022; Naughten et al., 2023). The economic costs of sea level rise are estimated at $40 billion per meter per year by 2100 (Brown et al., 2021). Furthermore, the social cost of mass migration away from the inundated coasts—around 200 million people per meter of sea level rise, and the ecological costs of destroyed wetlands, demands that research on all options be considered. These socio-economic costs are far larger than the costs associated with exploring many of the ideas (van Wijngaarden et al., 2024) proposed for stabilizing ice sheets. Ultimately, after urgent multi-disciplinary research ranging from ethics to engineering, one or more of these interventions may offer a better option than accepting the massive damages and consequences, especially in the Global South which will bear the brunt of sea level rise from ice sheet collapse (Brown et al., 2021).

Conflict of Interest

The authors declare no conflicts of interest relevant to this study.

Data Availability Statement

GeoMIP and CMIP5 data are available on the Earth System Grid Federation (https://esgf-node.llnl.gov/). The processed data used for analysis and figure drawing code are archived on zenodo (Moore et al., 2023).

Acknowledgments
We thank the climate modeling groups participating in the Geoengineering Model Intercomparison Project and their model development teams and the CLIVAR/WCRP Working Group on Coupled Modeling for endorsing the GeoMIP. This work was supported by National Key Research and Development Program of China (Grant 2021YFB3900105), and Academy of Finland (Grants 322430 and 355572).

References

Armstrong McKay, D. I., Staal, A., Abrams, J. F., Winkelmann, R., Sakschewski, B., Loriani, S., et al. (2022). Exceeding 1.5 C global warming could trigger multiple climate tipping points. *Science*, *377*(6611), eabn7950. https://doi.org/10.1126/science.abn7950

Assmann, K. M., Jenkins, A., Shoosmith, D. R., Walker, D. P., Jacobs, S. S., & Nicholls, K. W. (2013). Variability of circumpolar deep water transport onto the Amundsen Sea continental shelf through a shelf break trough. *Journal of Geophysical Research*, *118*(12), 6603–6620. https://doi.org/10.1002/2013JC008871

Azaneu, M., Webber, B., Heywood, K. J., Assmann, K. M., Dotto, T. S., & Abrahamsen, E. P. (2023). Influence of shelf break processes on the transport of warm waters onto the eastern Amundsen Sea continental shelf. *Journal of Geophysical Research: Oceans*, *128*(5), e2022JC019535. https://doi.org/10.1029/2022JC019535

Baldwin, M. P., & Dunkerton, T. J. (2001). Stratospheric harbingers of anomalous weather regimes. *Science*, *294*(5542), 581–584. https://doi.org/10.1126/science.1063315

Beadling, R. L., Russell, J. L., Stouffer, R. J., Mazloff, M., Talley, L. D., Goodman, P. J., et al. (2020). Representation of Southern Ocean Properties across Coupled Model Intercomparison Project Generations: CMIP3 to CMIP6. *Journal of Climate*, *33*(15), 6555–6581. https://doi.org/10.1175/jcli-d-19-0970.1

Benn, D. I., Luckman, A., Åström, J. A., Crawford, A. J., Cornford, S. L., Bevan, S. L., et al. (2022). Rapid fragmentation of Thwaites eastern ice shelf. *The Cryosphere*, *16*(6), 2545–2564. https://doi.org/10.5194/tc-16-2545-2022

Boucher, O., Servonnat, J., Albright, A. L., Aumont, O., Balkanski, Y., Bastrikov, V., et al. (2020). Presentation and evaluation of the IPSL-CM6A-LR climate model. *Journal of Advances in Modeling Earth Systems*, *12*(7), e2019MS002010. https://doi.org/10.1029/2019MS002010

Brown, S., Jenkins, K., Goodwin, P., Lincke, D., Vafeidis, A. T., Tol, R. S. J., et al. (2021). Global costs of protecting against sea-level rise at 1.5 to 4.0°C. *Climatic Change*, *167*(1–2), 4. https://doi.org/10.1007/s10584-021-03130-z

DeConto, R. M., & Pollard, D. (2016). Contribution of Antarctica to past and future sea-level rise. *Nature*, *531*(7596), 591–597. https://doi.org/10.1038/nature17145

Dotto, T. S., Naveira Garabato, A. C., Bacon, S., Holland, P. R., Kimura, S., Firing, Y. L., et al. (2019). Wind-driven processes controlling oceanic heat delivery to the Amundsen Sea, Antarctica. *Journal of Physical Oceanography*, *49*(11), 2829–2849. https://doi.org/10.1175/JPO-D-19-0064.1

Durand, G., Gagliardini, O., Favier, L., Zwinger, T., & le Meur, E. (2011). Impact of bedrock description on modeling ice sheet dynamics. *Geophysical Research Letters*, *38*(20), L20501. https://doi.org/10.1029/2011GL048892

Eyring, V., Arblaster, J. M., Cionni, I., Sedláček, J., Perlwitz, J., Young, P. J., et al. (2013). Long-term ozone changes and associated climate impacts in CMIP5 simulations. *Journal of Geophysical Research: Atmospheres*, *118*(10), 5029–5060. https://doi.org/10.1002/jgrd.50316

Favier, L., Durand, G., Cornford, S. L., Gudmundsson, G. H., Gagliardini, O., Gillet-Chaulet, F., et al. (2014). Retreat of Pine Island Glacier controlled by marine ice-sheet instability. *Nature Climate Change*, *4*(2), 117–121. https://doi.org/10.1038/nclimate2094

Gertler, C. G., O'Gorman, P. A., Kravitz, B., Moore, J. C., Phipps, S., & Watanabe, S. (2020). Weakening of the extratropical storm tracks in solar geoengineering scenarios. *Geophysical Research Letters*, *47*(11), e2020GL087348. https://doi.org/10.1029/2020GL087348

Gettelman, A., Hannay, C., Bacmeister, J. T., Neale, R. B., Pendergrass, A. G., Danabasoglu, G., et al. (2019). High climate sensitivity in the Community Earth System Model Version 2 (CESM2). *Geophysical Research Letters*, *46*(14), 8329–8337. https://doi.org/10.1029/2019GL083978

Gladstone, R., Galton-Fenzi, B., Gwyther, D., Zhou, Q., Hattermann, T., Zhao, C., et al. (2021). A framework for ice sheet - Ocean coupling (FISOC) V1.1. *Geoscientific Model Development*, *14*(2), 889–905. https://doi.org/10.5194/gmd-14-889-2021

Goddard, P. B., Kravitz, B., MacMartin, D. G., Visioni, D., Bednarz, E. M., & Lee, W. R. (2023). Stratospheric aerosol injection can reduce risks to Antarctic ice loss depending on injection location and amount. *Journal of Geophysical Research: Atmospheres*, *128*(22), e2023JD039434. https://doi.org/10.1029/2023JD039434

Govindasamy, B., Caldeira, K., & Duffy, P. (2003). Geoengineering earth's radiation balance to mitigate climate change from a quadrupling of CO_2. *Global and Planetary Change*, *37*(1), 157–168. https://doi.org/10.1016/S0921-8181(02)00195-9

Gutjahr, O., Putrasahan, D., Lohmann, K., Jungclaus, J. H., von Storch, J.-S., Brüggemann, N., et al. (2019). Max Planck Institute Earth System Model (MPI-ESM1.2) for the High-Resolution Model Intercomparison Project (HighResMIP). *Geoscientific Model Development*, *12*(7), 3241–3281. https://doi.org/10.5194/gmd-12-3241-2019

Harding, A. R., Ricke, K., Heyen, D., MacMartin, D. G., & Moreno-Cruz, J. (2020). Climate econometric models indicate solar geoengineering would reduce inter-country income inequality. *Nature Communications*, *11*(1), 227. https://doi.org/10.1038/s41467-019-13957-x

Hausfather, Z., Marvel, K., Schmidt, G. A., Nielsen-Gammon, J. W., & Zelinka, M. (2022). Climate simulations: Recognize the 'hot model' problem. *Nature*, *605*(7908), 26–29. https://doi.org/10.1038/d41586-022-01192-2

Heywood, K. J., Biddle, L. C., Boehme, L., Dutrieux, P., Fedak, M., Jenkins, A., et al. (2016). Between the devil and the deep blue sea: The role of the Amundsen Sea continental shelf in exchanges between ocean and ice shelves. *Oceanography*, *29*(4), 118–129. https://doi.org/10.5670/oceanog.2016.104

Hogan, K. A., Larter, R. D., Graham, A. G. C., Arthern, R., Kirkham, J. D., Totten Minzoni, R., et al. (2020). Revealing the former bed of Thwaites Glacier using sea-floor bathymetry: Implications for warm-water routing and bed controls on ice flow and buttressing. *The Cryosphere*, *14*(9), 2883–2908. https://doi.org/10.5194/tc-14-2883-2020

Holland, P. R., Bracegirdle, T. J., Dutrieux, P., Jenkins, A., & Steig, E. J. (2019). West Antarctic ice loss influenced by internal climate variability and anthropogenic forcing. *Nature Geoscience*, *12*(9), 718–724. https://doi.org/10.1038/s41561-019-0420-9

Irvine, P. J., & Keith, D. W. (2020). Halving warming with stratospheric aerosol geoengineering moderates policy-relevant climate hazards. *Environmental Research Letters*, *15*(4), 044011. https://doi.org/10.1088/1748-9326/ab76de

Jacobs, S. S., Jenkins, A., Giulivi, C. F., & Dutrieux, P. (2011). Stronger ocean circulation and increased melting under Pine Island Glacier ice shelf. *Nature Geoscience*, *4*(8), 519–523. https://doi.org/10.1038/ngeo1188

Jenkins, A., Dutrieux, P., Jacobs, S., Steig, E. J., Gudmundsson, G. H., Smith, J., & Heywood, K. J. (2016). Decadal ocean forcing and Antarctic ice sheet response: Lessons from the Amundsen Sea. *Oceanography*, *29*(4), 106–117. https://doi.org/10.5670/oceanog.2016.103

Joughin, I., Smith, B. E., & Medley, B. (2014). Marine ice sheet collapse potentially underway for the Thwaites Glacier Basin, West Antarctica. *Science*, *344*(6185), 735–738. https://doi.org/10.1126/science.1249055

Kitous, A., & Keramidas, K. (2015). *Analysis of scenarios integrating the INDCs*. European Commission.

Kravitz, B., Robock, A., Tilmes, S., Boucher, O., English, J. M., Irvine, P. J., et al. (2015). The Geoengineering Model Intercomparison Project Phase 6 (GeoMIP6): Simulation design and preliminary results. *Geoscientific Model Development*, *8*(10), 3379–3392. https://doi.org/10.5194/gmd-8-3379-2015

Lee, W. R., MacMartin, D. G., Visioni, D., & Kravitz, B. (2021). High-latitude stratospheric aerosol geoengineering can be more effective if injection is limited to spring. *Geophysical Research Letters*, *48*(9), e2021GL092696. https://doi.org/10.1029/2021GL092696

Liu, Y., Moore, J. C., Cheng, X., Gladstone, R. M., Bassis, J. N., Liu, H., et al. (2015). Ocean-driven thinning enhances iceberg calving and retreat of Antarctic ice shelves. *Proceedings of the National Academy of Sciences*, *112*(11), 3263–3268. https://doi.org/10.1073/pnas.1415137112

Mauritsen, T., Bader, J., Becker, T., Behrens, J., Bittner, M., Brokopf, R., et al. (2019). Developments in the MPI-M Earth System Model version 1.2 (MPI-ESM1.2) and its response to increasing CO_2. *Journal of Advances in Modeling Earth Systems*, *11*(4), 998–1038. https://doi.org/10.1029/2018MS001400

McCusker, K. E., Battisti, D. S., & Bitz, C. M. (2015). Inability of stratospheric sulfate aerosol injections to preserve the West Antarctic ice sheet. *Geophysical Research Letters*, *42*(12), 4989–4997. https://doi.org/10.1002/2015gl064314

Meehl, G. A., Senior, C. A., Eyring, V., Flato, G., Lamarque, J. F., Stouffer, R. J., et al. (2020). Context for interpreting equilibrium climate sensitivity and transient climate response from the CMIP6 Earth system models. *Science Advances*, *6*(26), eaba1981. https://doi.org/10.1126/sciadv.aba1981

Moore, J. C., Yue, C., Chen, Y., Jevrejeva, S., Visioni, D., Uotila, P., & Zhao, L. (2023). Dataset for "Multi-model simulation of solar geo-engineering indicates avoidable destabilization of the West Antarctic ice sheet" [Dataset]. *Zenodo*. https://doi.org/10.5281/zenodo.10479013

Morlighem, M., Rignot, E., Binder, T., Blankenship, D., Drews, R., Eagles, G., et al. (2020). Deep glacial troughs and stabilizing ridges unveiled beneath the margins of the Antarctic ice sheet. *Nature Geoscience*, *13*(2), 132–137. https://doi.org/10.1038/s41561-019-0510-8

Naughten, K. A., Holland, P. R., & De Rydt, J. (2023). Unavoidable future increase in West Antarctic ice-shelf melting over the twenty-first century. *Nature Climate Change*, *13*(11), 1222–1228. https://doi.org/10.1038/s41558-023-01818-x

Niemeier, U., & Schmidt, H. (2017). Changing transport processes in the stratosphere by radiative heating of sulfate aerosols. *Atmospheric Chemistry and Physics*, *17*(24), 14871–14886. https://doi.org/10.5194/acp-17-14871-2017

O'Neill, B. C., Tebaldi, C., van Vuuren, D. P., Eyring, V., Friedlingstein, P., Hurtt, G., et al. (2016). The scenario model lntercomparison project (ScenarioMIP) for CMIP6. *Geoscientific Model Development*, *9*, 3461–3482. https://doi.org/10.5194/gmd-9-3461-2016

Rezaei, A., Karami, K., Tilmes, S., & Moore, J. C. (2023). Changes in global teleconnection patterns under global warming and stratospheric aerosol intervention scenarios. *Atmospheric Chemistry and Physics*, *23*(10), 5835–5850. https://doi.org/10.5194/acp-23-5835-2023

Rignot, E., & Jacobs, S. S. (2002). Rapid bottom melting widespread near Antarctic ice sheet grounding lines. *Science*, *296*(5575), 2020–2023. https://doi.org/10.1126/science.1070942

Rignot, E., Mouginot, J., Morlighem, M., Seroussi, H., & Scheuchl, B. (2014). Widespread, rapid grounding line retreat of Pine Island, Thwaites, Smith and Kohler glaciers, West Antarctica from 1992 to 2011. *Geophysical Research Letters*, *41*(10), 3502–3509. https://doi.org/10.1002/2014gl060140

Rintoul, S. R., & Naveira Garabato, A. C. (2013). Chapter 18 - Dynamics of the Southern Ocean circulation. In G. Siedler, S. M. Griffies, J. Gould, & J. A. Church (Eds.), *International geophysics* (Vol. 103, pp. 471–492). Academic Press. https://doi.org/10.1016/B978-0-12-391851-2.00018-0

Robock, A. (2000). Volcanic eruptions and climate. *Reviews of Geophysics*, *38*(2), 191–219. https://doi.org/10.1029/1998rg000054

Schoof, C. (2007). Ice sheet grounding line dynamics: Steady states, stability, and hysteresis. *Journal of Geophysical Research: Earth Surface*, *112*(F3), F03S28. https://doi.org/10.1029/2006jf000664

Séférian, R., Nabat, P., Michou, M., Saint-Martin, D., Voldoire, A., Colin, J., et al. (2019). Evaluation of CNRM Earth System Model, CNRM-ESM2-1: Role of earth system processes in present-day and future climate. *Journal of Advances in Modeling Earth Systems*, *11*(12), 4182–4227. https://doi.org/10.1029/2019MS001791

Sellar, A. A., Jones, C. G., Mulcahy, J. P., Tang, Y., Yool, A., Wiltshire, A., et al. (2019). UKESM1: Description and evaluation of the U.K. Earth system model. *Journal of Advances in Modeling Earth Systems*, *11*(12), 4513–4558. https://doi.org/10.1029/2019MS001739

Spence, P., Griffies, S. M., England, M. H., Hogg, A. M. C., Saenko, O. A., & Jouradin, N. C. (2014). Rapid subsurface warming and circulation changes of Antarctic coastal waters by poleward shifting winds. *Geophysical Research Letters*, *41*(13), 4601–4610. https://doi.org/10.1002/2014GL060613

Sutter, J., Jones, A., Frölicher, T. L., Wirths, C., & Stocker, T. F. (2023). Climate intervention on a high-emissions pathway could delay but not prevent West Antarctic Ice Sheet demise. *Nature Climate Change*, *13*(9), 951–960. https://doi.org/10.1038/s41558-023-01738-w

Thoma, M., Jenkins, A., Holland, D., & Jacobs, S. (2008). Modelling circumpolar deep water intrusions on the Amundsen Sea continental shelf, Antarctica. *Geophysical Research Letters*, *35*(18), L18602. https://doi.org/10.1029/2008GL034939

Tilmes, S., Mills, M. J., Niemeier, U., Schmidt, H., Robock, A., Kravitz, B., et al. (2015). A new Geoengineering Model Intercomparison Project (GeoMIP) experiment designed for climate and chemistry models. *Geoscientific Model Development*, *8*(1), 43–49. https://doi.org/10.5194/gmd-8-43-2015

Tilmes, S., Visioni, D., Jones, A., Haywood, J., Séférian, R., Nabat, P., et al. (2022). Stratospheric ozone response to sulfate aerosol and solar dimming climate interventions based on the G6 Geoengineering Model Intercomparison Project (GeoMIP) simulations. *Atmospheric Chemistry and Physics*, *22*(7), 4557–4579. https://doi.org/10.5194/acp-22-4557-2022

Trenberth, K., Fasullo, J., von Schuckmann, K., & Cheng, L. (2016). Insights into earth's energy imbalance from multiple sources. *Journal of Climate*, *29*(20), 7495–7505. https://doi.org/10.1175/JCLI-D-16-0339.1

Turner, J., Orr, A., Gudmundsson, G. H., Jenkins, A., Bingham, R. G., Hillenbrand, C.-D., & Bracegirdle, T. J. (2017). Atmosphere-ocean-ice interactions in the Amundsen Sea Embayment, West Antarctica. *Reviews of Geophysics*, *55*(1), 235–276. https://doi.org/10.1002/2016RG000532

Vallis, G. (2017). *Atmospheric and oceanic fluid dynamics: Fundamentals and large-scale circulation (2nd ed., chapter 20)*. Cambridge University Press. https://doi.org/10.1017/9781107588417

van Wijngaarden, A., Moore, J. C., Alfthan, B., Kurvits, T., & Kullerud, L. (2024). A survey of interventions to actively conserve the frozen North. *Climatic Change*, *177*(4), 58. https://doi.org/10.1007/s10584-024-03705-6

Visioni, D., Kravitz, B., Robock, A., Tilmes, S., Haywood, J. M., Boucher, O., et al. (2023). Opinion: The scientific and community-building roles of the Geoengineering Model Intercomparison Project (GeoMIP) - Past, present, and future. *Atmospheric Chemistry and Physics*, *23*(9), 5149–5176. https://doi.org/10.5194/acp-23-5149-2023

Visioni, D., MacMartin, D. G., Kravitz, B., Boucher, O., Jones, A., Lurton, T., et al. (2021). Identifying the sources of uncertainty in climate model simulations of solar radiation modification with the G6sulfur and G6solar Geoengineering Model Intercomparison Project (GeoMIP) simulations. *Atmospheric Chemistry and Physics*, *21*(13), 10039–10063. https://doi.org/10.5194/acp-21-10039-2021

Visioni, D., MacMartin, D. G., Kravitz, B., Lee, W., Simpson, I. R., & Richter, J. H. (2020). Reduced poleward transport due to stratospheric heating under stratospheric aerosols geoengineering. *Geophysical Research Letters*, *47*(17), e2020GL089470. https://doi.org/10.1029/2020GL089470

Wåhlin, A., Queste, B., Graham, A., Hogan, K., Brohme, L., Heywood, K., et al. (2020). *Warm water flow and mixing beneath Thwaites Glacier ice shelf, West Antarctica*. Online. https://doi.org/10.5194/egusphere-egu2020-19934

Wåhlin, A. K., Kalén, O., Arneborg, L., Björk, G., Carvajal, G. K., Ha, H. K., et al. (2013). Variability of warm deep water inflow in a submarine trough on the Amundsen Sea shelf. *Journal of Physical Oceanography*, *43*(10), 2054–2070. https://doi.org/10.1175/JPO-D-12-0157.1

Walker, D. P., Jenkins, A., Assmann, K. M., Shoosmith, D. R., & Brandon, M. A. (2013). Oceanographic observations at the shelf break of the Amundsen Sea, Antarctica. *Journal of Geophysical Research*, *118*(6), 2906–2918. https://doi.org/10.1002/jgrc.20212

Wei, L., Ji, D., Miao, C., Muri, H., & Moore, J. C. (2018). Global streamflow and river discharge under stratospheric aerosol geoengineering. *Atmospheric Chemistry and Physics*, *18*(21), 16033–16050. https://doi.org/10.5194/acp-18-16033-2018

Wieners, C. E., Hofbauer, B. P., de Vries, I. E., Honegger, M., Visioni, D., Russchenberg, H. W., & Felgenhauer, T. (2023). Solar radiation modification is risky, but so is rejecting it: A call for balanced research. *Oxford Open Climate Change*, *3*(1), kgad002. https://doi.org/10.1093/oxfclm/kgad002

Xie, M., Moore, J. C., Zhao, L., Wolovick, M., & Muri, H. (2022). Impacts of three types of solar geoengineering on the Atlantic meridional overturning circulation. *Atmospheric Chemistry and Physics*, *22*(7), 4581–4597. https://doi.org/10.5194/acp-22-4581-2022

Yue, C., Jevrejeva, S., Qu, Y., Zhao, L., & Moore, J. C. (2023). Thermosteric and dynamic sea level under solar geoengineering. *npj Climate and Atmospheric Science*, *6*(1), 135. https://doi.org/10.1038/s41612-023-00466-4

References From the Supporting Information

Gupta, A. S., Jourdain, N. C., Brown, J. N., & Monselesan, D. (2013). Climate drift in the CMIP5 models. *Journal of Climate*, *26*(21), 8597–8615. https://doi.org/10.1175/JCLI-D-12-00521.1

Slangen, A. B. A., Katsman, C. A., Van de Wal, R. S. W., Vermeersen, L. L. A., & Riva, R. E. M. (2012). Towards regional projections of twenty-first century sea-level change based on IPCC SRES scenarios. *Climate Dynamics*, *38*(5–6), 1191–1209. https://doi.org/10.1007/s00382-011-1057-6